metals

MDPI

Article

Effect of Magnet Alternate Stirring on the Internal Quality of Sn-Pb Alloy

Mengyun Zhang, Yanping Bao * and Haibo Zhang

State Key Laboratory of Advanced Metallurgy, University of Science and Technology Beijing, Beijing 100083, China; b20190545@xs.ustb.edu.cn (M.Z.)
* Correspondence: baoyp@ustb.edu.cn

Abstract: A permanent magnet stirrer was built to study the effect of different magnetic field stirring modes on the solidification quality of Sn-20 wt-% Pb alloy ingots. The internal quality of the ingot can be improved by adjusting both the stirring speed and the modes. When the continuous magnetic stirring mode was adopted, the higher the stirring speed, the higher the flutter height at the ingot edge. When the stirring speed was 200 rpm, the flutter height reached 4.12 mm. The rotating magnetic field can significantly refine the grain size of the ingot. When the stirring speed of the magnetic field was increased from 0 rpm to 200 rpm, the grain size of the ingot reduced from 301 μm to 241 μm. By fixing the magnetic field stirring speed to 200 rpm and adjusting the mode to the alternate stirring process, the flutter height at the ingot edge reduced to 1.86 mm, which stabilized the liquid level of the molten alloy in the crucible. In addition, the grain size of the ingot was shortened to 223 μm, and the elemental homogeneity within the ingot was optimized.

Keywords: permanent magnetic stirring; Sn-Pb alloy; alternate stirring mode; ingot morphology; solidification quality; element segregation

check for updates

Citation: Zhang, M.; Bao, Y.; Zhang, H. Effect of Magnet Alternate Stirring on the Internal Quality of Sn-Pb Alloy. *Metals* **2023**, *13*, 1732. https://doi.org/10.3390/met13101732

Received: 23 August 2023
Revised: 21 September 2023
Accepted: 3 October 2023
Published: 12 October 2023

Copyright: © 2023 by the authors. Licensee MDPI, Basel, Switzerland. This article is an open access article distributed under the terms and conditions of the Creative Commons Attribution (CC BY) license (https://creativecommons.org/licenses/by/4.0/).

1. Introduction

With the increasing requirements of customers for steel quality, it is particularly important to provide defect-free continuous casting billet. The quality of billet includes two types: external and internal quality, and common defects mainly include cracks, shrinkage cavities, and segregation [1–4]. At present, in order to improve the quality of the billet, the process of continuous casting mainly involves controlling the temperature of molten steel in the tundish, supplemented with electromagnetic stirring and soft reduction processes [5–8]. Round billet is one of the main raw materials for producing seamless pipes because of its special cross-sectional shape. Due to the requirements for the ovality of round billets in the pipe threading process, the production process of round billets is generally not installed with soft reduction equipment, but mainly through electromagnetic stirring technology to improve the quality of billets [9,10].

Electromagnetic stirring technology is mainly divided into three types: mold, secondary cooling, and final electromagnetic stirring [11–13]. Although there are differences in the location and purpose of the above electromagnetic stirring processes, most scholars have shown that the application of electromagnetic stirring to the steel during continuous casting can significantly improve the internal quality of the billet [14–17]. The principle is mainly that the electromagnetic force applied to the high-temperature molten steel can greatly improve temperature and flow field, thereby reducing the superheat of the molten steel and distributing the concentrated elements [18,19]. The internal quality of the billet is mainly composed of the solidification structure and element segregation, as the above two defects are easily inherited into the pipe during the hot rolling process, thereby affecting the stability of the product [20–23]. Therefore, it is particularly important to identify an electromagnetic stirring mode that can simultaneously improve the internal quality of the billet.

At present, the production of continuous casting billets is considerable. If industrial experiments are conducted directly, it may cause significant quality fluctuations in the continuous casting process due to unsuitable parameter selection, thereby deteriorating the production quality. Based on the above reasons, an experimental permanent magnet stirrer (PMS) was developed and the magnetic field was generated using a pair of NdFeB permanent magnets. The effect of different magnetic stirring modes on the quality of ingots was studied by selecting Sn-20 wt-% Pb alloy instead of high-temperature molten steel. In this paper, solidification experiments were conducted on alloy ingots under different magnetic stirring modes. By detecting and comparing the macroscopic morphology, solidification structure, and element segregation of the samples, the differences between the different magnetic stirring modes were quantitatively evaluated, and the improvement effect of the magnetic alternate stirring mode on ingot quality could be clarified. The above results provide theoretical support for the implementation of subsequent industrial experiments.

2. Experimental Section

2.1. Construction of PMS

In order to systematically study the effect of different magnetic field stirring modes on the internal quality of ingots, a permanent magnetic stirrer was developed. Figure 1 shows the schematic diagram and actual installation diagram of the PMS. The PMS mainly consists of three parts: the permanent magnet, the rotating support device, and the equipment frame. The NdFeB permanent magnet was selected as the magnetic field source, and the permanent magnet was driven to rotate by a motor, thus imitating the electromagnetic magnetic field in industrial production.

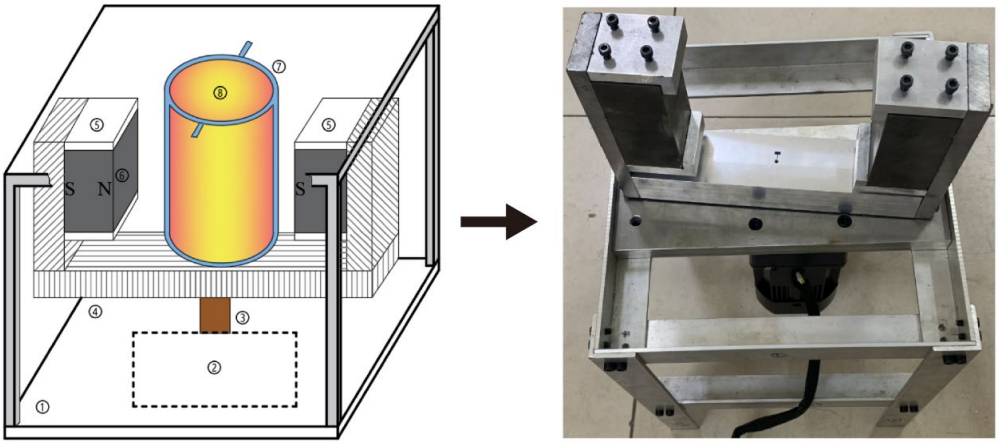

Figure 1. Schematic diagram and actual installation diagram of the PMS: ① equipment frame; ② rotating electrical machines; ③ rotating bearing; ④ magnetic yoke; ⑤ aluminum block; ⑥ permanent magnets; ⑦ cooling copper pipe; ⑧ crucible.

The equipment frame was constructed of aluminum alloy to stabilize the experimental equipment. The upper part was welded with a copper groove of suitable size, while the insulation cotton was embedded, which stabilizes the crucible during the experiment and can prevent excessive diffusion of high temperature outward, thereby reducing the magnetism of the permanent magnet. The rotating device mainly includes a rotating motor, rotating bearings, and a magnetic yoke. The rotating motor can ensure a maximum rotational speed of 300 rpm at a load of 30 kg and can achieve an alternating rotation of the magnetic field. The yoke is made of pure iron and can be used as a transmission route for magnetic induction lines.

2.2. Selection of Permanent Magnets

Permanent magnets should have high coercive force, residual magnetization, and other properties. In this study, the magnetic field was generated using a pair of N38H-

series NdFeB permanent magnets, with a residual magnetization Br of about 1.23 T and a maximum operating temperature of 120 °C. During installation, the N and S poles are placed opposite each other to ensure that the completed magnetic field is generated.

To directly observe the magnetic field distribution between the permanent magnets, a KANETEC TM-701-type Gauss meter was used to measure the magnetic intensity at different positions within the crucible. A schematic diagram of the magnetic field measurement for the permanent magnet stirrer is shown in Figure 2. For the measurement of the magnetic field, the magnetic intensity was measured at 5 mm intervals starting from one side of the longitudinal center surface of the crucible to the other side, for a total of 11 measurement points. The test results are shown in Figure 3.

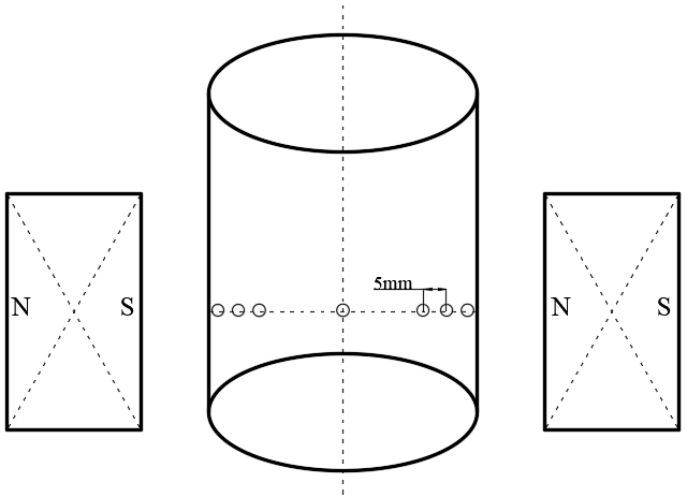

Figure 2. Schematic diagram of magnetic field measurement for permanent magnet stirrer.

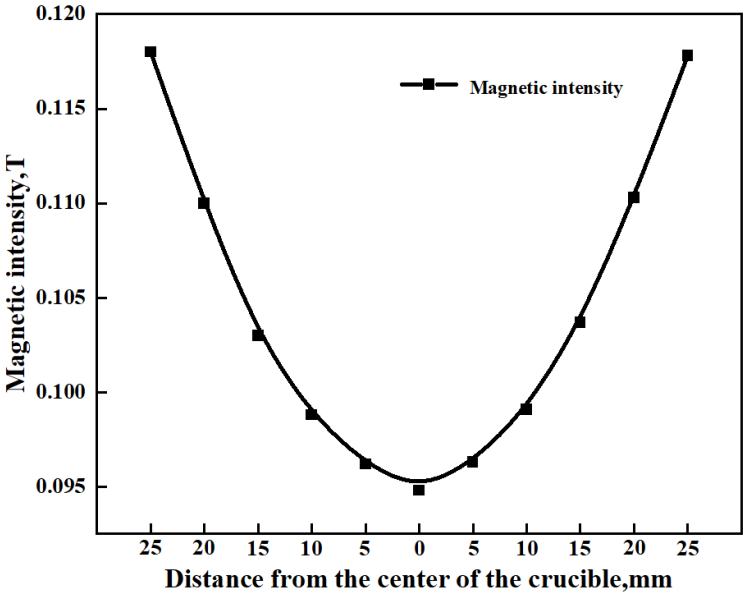

Figure 3. Schematic diagram of magnetic field measurement results.

For the measurement of the magnetic field, the magnetic intensity was measured at 5 mm intervals starting from one side of the longitudinal center surface of the crucible to the other side, for a total of 11 measurement points. The test results are shown in Figure 3.

As shown in Figure 3, the magnetic intensity increased gradually as the Gauss meter probe moved from the center to the edge of the crucible. The magnetic intensity at the center of the crucible was about 948 GS, and the edge position was about 1179 GS. It is well known that electromagnetic stirring equipment can control the magnetic force by adjusting

the stirring current and frequency. However, due to the fixed magnetic intensity, the PMS mainly controls the magnetic force by adjusting the stirring speed of the magnet.

2.3. Selection of Alloy

For the selection of an alloy, it is necessary to ensure that the alloy is melting at a low temperature (melting point less than 300 °C), and that its properties are similar to those of steel. In this study, a Sn-Pb alloy with a mass fraction ratio of 80%:20% was selected instead of steel. Table 1 shows the comparison of the material properties between Sn-20 wt-% Pb alloy and GCr15 steel.

Table 1. Comparison of material properties between alloy and steel.

Material Properties	Sn-20 wt-% Pb Alloy	GCr15 Steel
Liquid temperature/°C	206	1467
Solidus temperature/°C	183	1366
Density/kg·m^{-3}	7860	7200
Electrical conductivity/1·(Ω·m)$^{-1}$	1.90×10^{6}	7.14×10^{5}
Kinematic viscosity/m^{2}·s^{-1}	3.02×10^{-7}	5.72×10^{-7}

The Sn-20 wt-% Pb alloy was prepared using Sn alloy and Pb alloy with a purity of 99.9%. The weighed Sn and Pb alloy were placed into an alumina crucible in proportion; then, an induction furnace was used to heat them to 350 °C and was held for 30 min to allow the temperature in the crucible to be uniform. The crucible containing molten alloy was placed in the center of the PMS, and the entire process was subjected to radiant heat exchange with the surrounding environment. The size of the Sn-Pb ingot was approximately Φ50 mm × 60 mm.

2.4. Preparation of Experiments

As is known, increasing the intensity of electromagnetic stirring in the mold can accelerate the superheat dissipation of high-temperature molten steel, thereby increasing the proportion of equiaxed grain in the core of the billet [24,25]. Theoretically, the greater the magnetic intensity in the mold, the better the internal quality of the billet. Nevertheless, with an increase in the magnetic intensity, the quality of the billet will also deteriorate, such as the formation of white bands in the billet, reducing the stability of the steel level in the mold and increasing the risk of slag entrapment in the molten steel [26,27]. When the magnetic field adopts an alternate stirring mode, which can stabilize the steel level in the mold to a certain extent due to continuous changes in the stirring direction, it is possible to set a greater electromagnetic stirring force than continuous stirring.

To ensure complete solidification of the molten alloy in the crucible during the experimental process, the stirring time was set to 60 min. For the determination of the forward and backward stirring time under the magnetic alternate field stirring mode, a numerical simulation method was used to calculate the time it takes for the molten alloy in the crucible to reach a stable speed under different magnetic field speeds, as shown in Figure 4. When the magnetic field speed was set to 200 rpm, stirring for 6.75 s stabilized the alloy speed in the crucible, so the forward and backward stirring time was set to 7 s. During the experiment, after stopping stirring for 5 s, the speed of the molten alloy reached zero, so the stop stirring time was set to 5 s. In order to systematically study the effects of different stirring speeds and modes on the internal quality of the ingot during solidification, a corresponding test program was designed, as shown in Table 2.

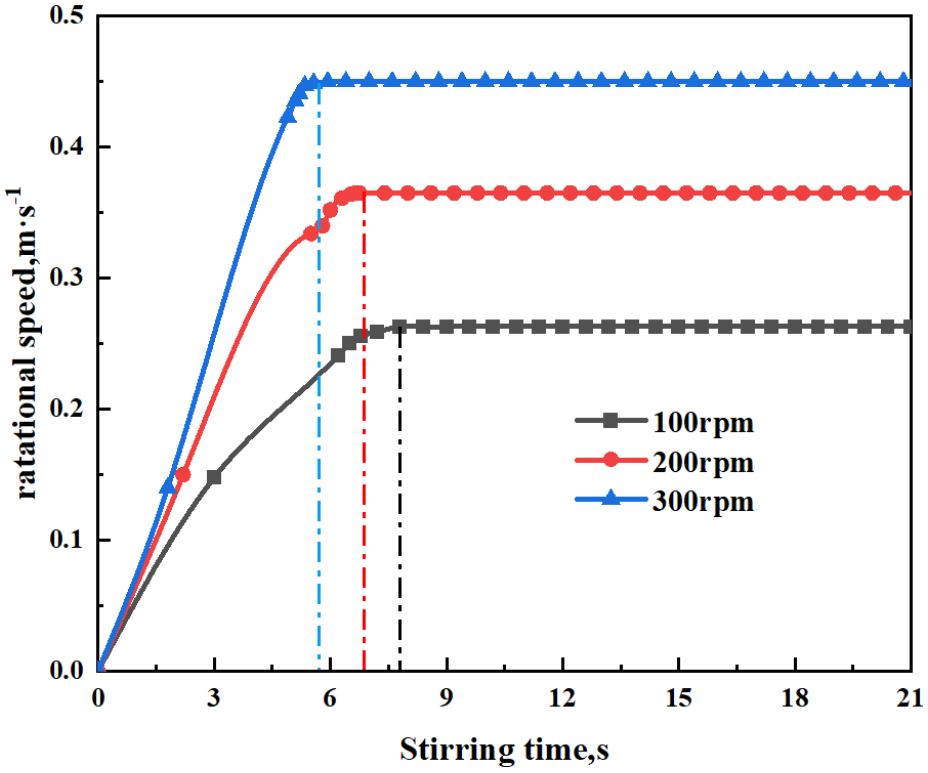

Figure 4. Relationship between the rotational speed of molten alloy and stirring time.

Table 2. Test scheme of magnetic stirring modes.

No.	Stirring Mode	Stirring Speed/rpm	Stirring Time
1	PMS—NO	0	0
2	PMS—CS	100	60 min
3	PMS—CS	200	60 min
4	PMS—AS	200	7 s–5 s–7 s, 60 min

PMS-CS: continuous stirring; PMS-AS: alternate stirring.

3. Detection of Test Samples

3.1. Detection of Solidification Structure

In order to clarify the effect of different stirring modes on the internal quality of the ingot, transverse and longitudinal samples were taken for observation and analysis of the solidification structure. The schematic diagram of sample processing and testing is shown in Figure 5. In the longitudinal direction, the ingot was cut into two parts with a thickness of 10 mm and 50 mm. The upper cross-sectional samples were used to observe the macroscopic morphology using a camera (Canon D60, Canon Japan, Tokyo, Japan), and the lower sample was cut along the center of the longitudinal section. After the longitudinal samples were polished, the polished surface was etched using an acid solution (2 mL of HCL, 10 g of $FeCl_3$, and 100 mL of H_2O) and observed using a metallographic microscope (Leica DM4M, Leica Germany, Wetzlar, Germany).

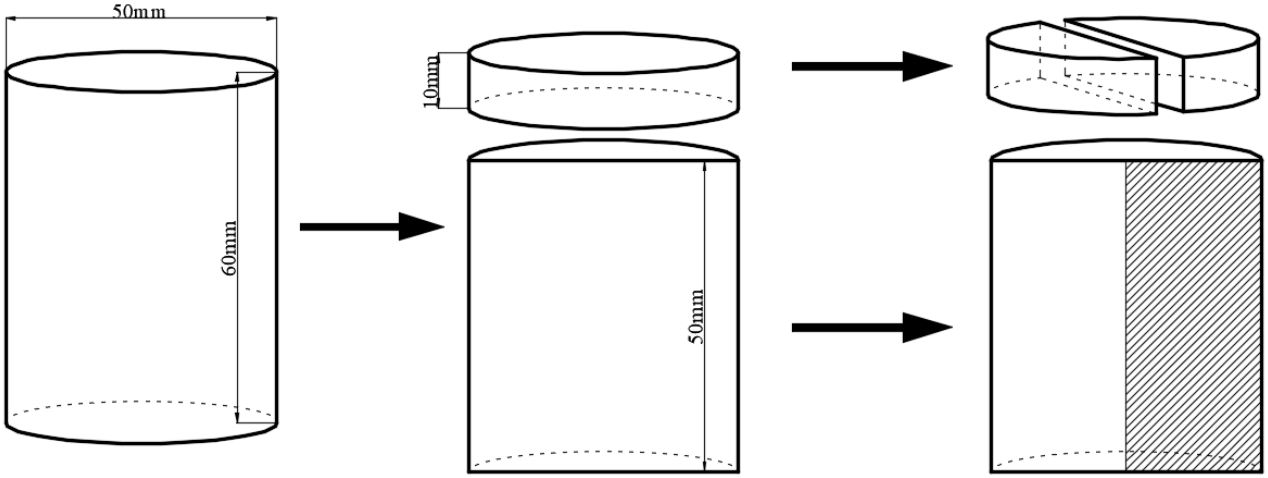

Figure 5. Schematic diagram of sample processing and testing.

3.2. Detection of Element Uniformity

To further clarify the influence of different magnetic stirring modes on the element uniformity of the alloy ingots, the Sn element content at a different position in the cross- and longitudinal section of the ingots was detected using a SHIMADZU EDX-8000 X-ray fluorescence spectrometer (XRF). The XRF detection was a circle with a diameter of 5 mm, and the spacing between the detection points was 10 mm. Each measurement point was tested three times, and the average value was taken as the result at this location. The location of the detection point is shown in Figure 6. The cross-section is H1 to H5 from left to right, and the center point is H3. The longitudinal section is Z1 to Z5 from top to bottom, and the center point is Z3.

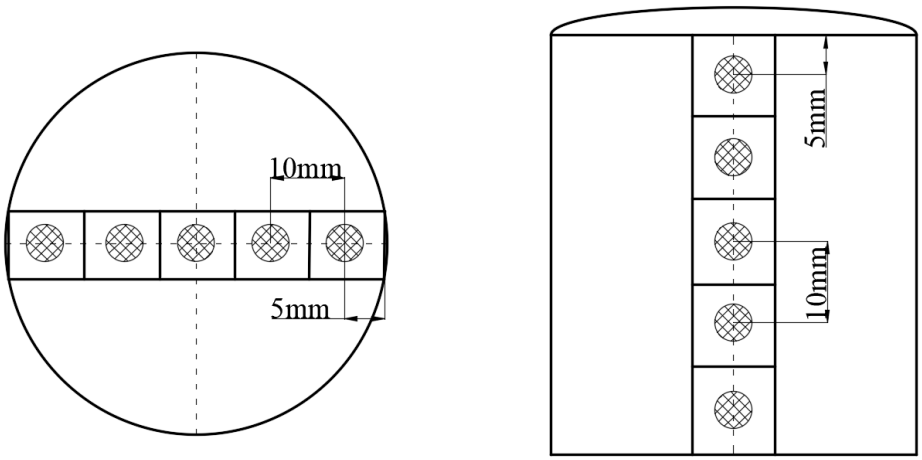

Figure 6. Schematic diagram of element detection points of ingots.

4. Results and Discussion

4.1. Top Morphology of Ingots

In this paper, the magnetic field was fixed, and the solidification process of the alloy was affected by adjusting the stirring speed and modes of the permanent magnet. This section mainly observed the top morphology of the ingots and quantitatively analyzed the stability of the molten alloy in the crucible during solidification under different magnetic field stirring modes. Figure 7 shows the top morphology of the ingots under different magnetic field stirring modes.

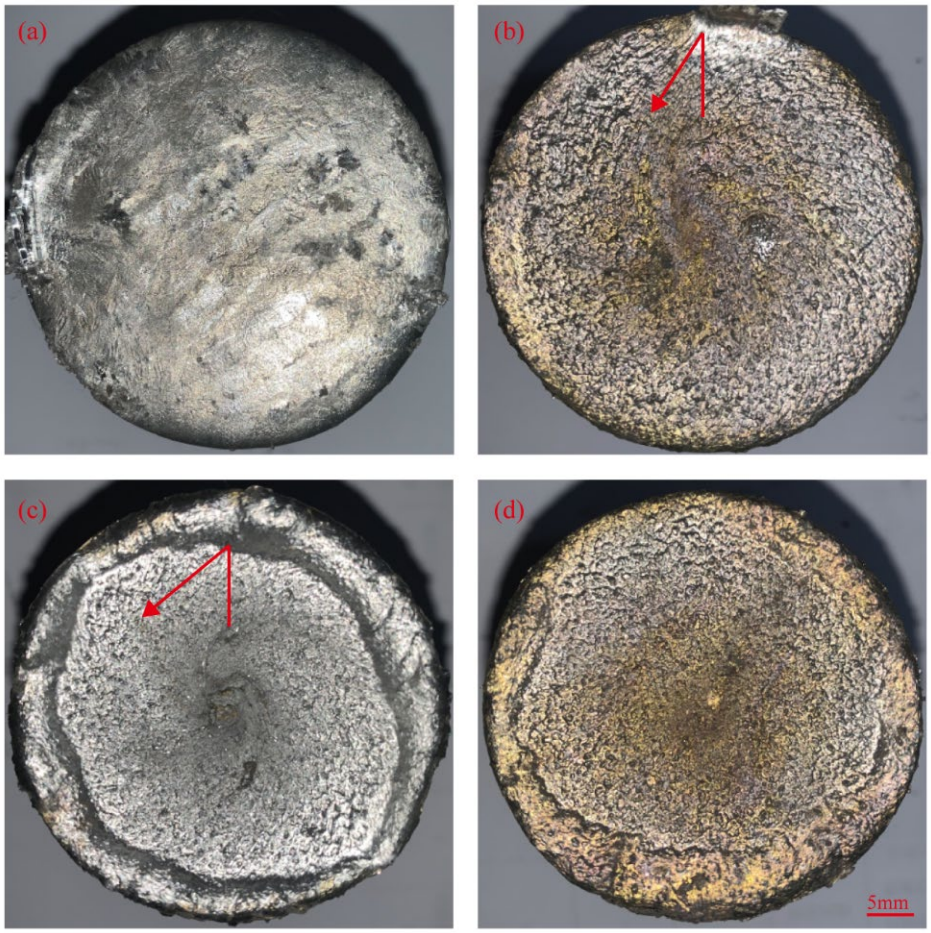

Figure 7. Top morphology of ingots under different magnetic field stirring modes: (**a**) 0 rpm; (**b**) continuous stirring, 100 rpm; (**c**) continuous stirring, 200 rpm; (**d**) alternate stirring, 200 rpm.

It can be seen from Figure 7 that when the magnetic field was stationary, the top of the alloy after solidification was a typical ingot morphology without a rotating streamline. In the continuous stirring mode, there are obvious signs of rotation on the top of the ingots after solidification, and the alloy rotation direction is consistent with the rotation direction of the permanent magnet. As the magnetic stirring speed increased from 100 rpm to 200 rpm, the solidification streamline of the ingots increased from 32° to 47°. When the magnetic field stirring speed was fixed at 200 rpm and the alternate stirring mode was adopted, there was no obvious rotation trace on the top of the ingot after solidification, but only a certain fluctuation trace.

Figure 8 shows the flutter morphology of the edge of the ingots under different magnetic field stirring modes. The flutter height of the ingots under different magnetic field stirring modes is shown in Table 3.

Table 3. Flutter height of ingots under different stirring modes.

Stirring Mode	Continuous Stirring			Alternate Stirring
Stirring speed/rpm	0	100	200	200
Flutter height/mm	0	1.12	4.12	1.86

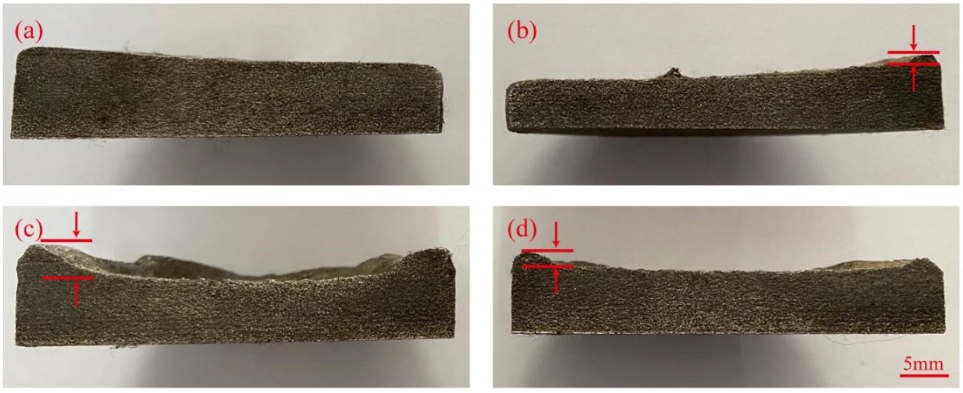

Figure 8. Flutter morphology of ingots under different stirring modes: (**a**) 0 rpm; (**b**) continuous stirring, 100 rpm; (**c**) continuous stirring, 200 rpm; (**d**) alternate stirring, 200 rpm.

According to the analysis of Figure 8 and Table 3, when the magnetic field was stationary (the rotating speed was 0 rpm), the molten alloy in the crucible also remained stationary during solidification, so the flutter height at the edge of the ingot was 0 mm. When the magnetic field continuous stirring mode was adopted and the stirring speed was 100 rpm and 200 rpm, the flutter height of the ingots was 1.12 mm and 4.12 mm, respectively. When the magnetic field stirring speed was fixed at 200 rpm and the alternate stirring mode was adopted, the flutter height of the ingot was reduced to 1.86 mm. From the above comparison, it can be seen that after using the alternate stirring mode, the magnetic field can stabilize the molten alloy in the crucible to a certain extent due to the periodic change in the magnetic field rotation direction.

4.2. Solidification Morphology of Ingots

The periodic motion of the magnetic field can drive the flow of molten alloy in the crucible, thus forming a larger temperature gradient and improving the release of internal heat. At the same time, the rotating molten alloy can scour the dendrites at the solidification front, thus forming a large number of fractured dendrites. These fractured dendrites, on the one hand, move to the core of the billet to further lower the temperature via remelting; on the other hand, they provide conditions for the growth of central equiaxed crystal as nucleate particles. Under the action of the above two aspects, the rotation of the magnetic field can refine the grains during the solidification process of the molten alloy, thereby improving the solidification structure of the ingots. Figure 9 shows the solidification structure of the local area in the longitudinal section of the ingots under different stirring modes.

It can be seen from Figure 9 that when the magnetic field was stationary, the solidification structure on the longitudinal section of the ingot was dominated by a long-size dendritic morphology. This phenomenon indicates that during the solidification process, the molten alloy in the crucible forms a higher temperature gradient with the environment, providing conditions for the growth of columnar crystals. As the magnetic field begins to move, the molten alloy in the crucible gradually moves with the change in the magnetic field. The moving molten alloy cuts the solidified dendrites, hindering their growth trend towards the center of the ingot, thus reducing the length of the solidified dendrites and turning them into short and coarse dendrites.

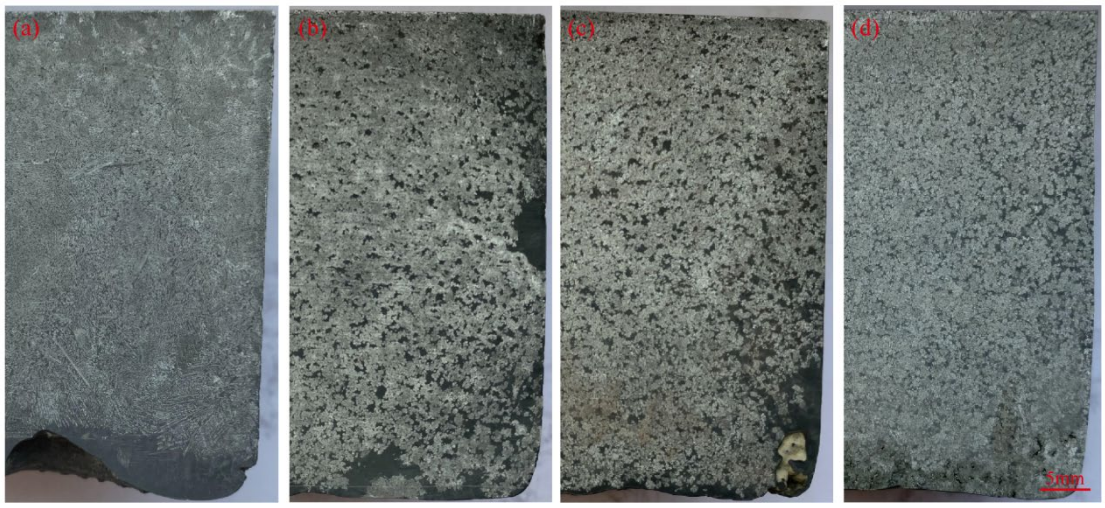

Figure 9. Solidification structure of local area in the longitudinal section of the ingots under different stirring modes: (**a**) 0 rpm; (**b**) continuous stirring, 100 rpm; (**c**) continuous stirring, 200 rpm; (**d**) alternate stirring, 200 rpm.

As an easy segregation element, the Pb element is easy to precipitate between grains [28,29]. The erosion solution reacts with the Pb element to make its surface rough, thus resulting in a grayish black color under an optical microscope, while conversely, it is a grain formed by Sn. By comparing the typical grain morphology in the solidification structure, the influence of different magnetic field stirring modes on the internal quality of the ingots was quantitatively analyzed. Figure 10 shows typical grain morphology in various samples under different stirring modes.

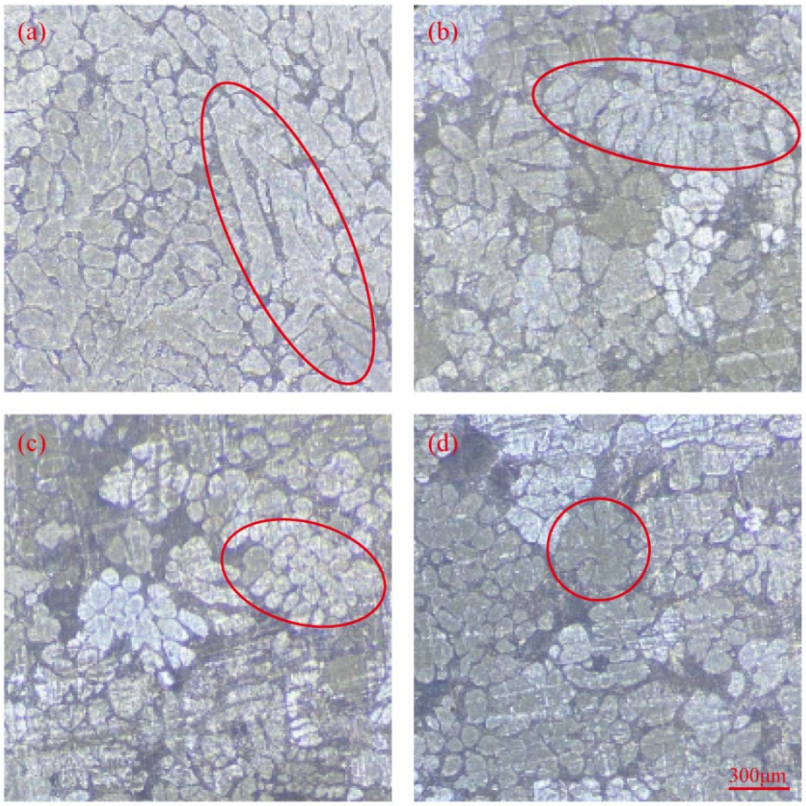

Figure 10. Typical grain morphology under different stirring modes: (**a**) 0 rpm; (**b**) continuous stirring, 100 rpm; (**c**) continuous stirring, 200 rpm; (**d**) alternate stirring, 200 rpm.

It can be seen from the comparison in Figure 10 that when the magnetic field was stationary, there were large columnar crystals inside the ingot. When the continuous stirring mode was adopted for the magnetic field, fractured columnar crystals could still be found in the samples, and the size of the columnar crystals decreased significantly with the increase in the stirring speed. When the stirring speed was 200 rpm and the alternate stirring was adopted for the magnetic field, the elongated dendrites in the sample were eliminated, and only cluster dendrites could be observed. Typical dendritic morphology under different magnetic field stirring modes is shown in the red circles in Figure 10.

In this article, the Image-Pro Plus 6.0 software was used to obtain quantitative statistics on the grain size of the samples under different stirring modes. The statistical method involved selecting 10 groups of grains from each sample for size measurement and taking the average value as the grain size of the corresponding sample. The statistical results are shown in Figure 10. According to Figure 11, when the magnetic field was stationary, the maximum grain size in the ingot was about 301 μm. As the magnetic field moves circumferentially along the crucible, the higher the stirring speed, the smaller the grain size. When the stirring speed was 100 rpm and 200 rpm, the grain size of the ingot samples was 279 μm and 241 μm, respectively. When the alternate stirring mode was adopted for the magnetic field and the stirring speed was set at 200 rpm, the grain size of the sample was about 223 μm. This is the smallest of the four magnetic field stirring modes. That is, when the magnetic field was in the alternate stirring mode, the grain size in the ingot was the smallest and the compactness of the ingot was the best.

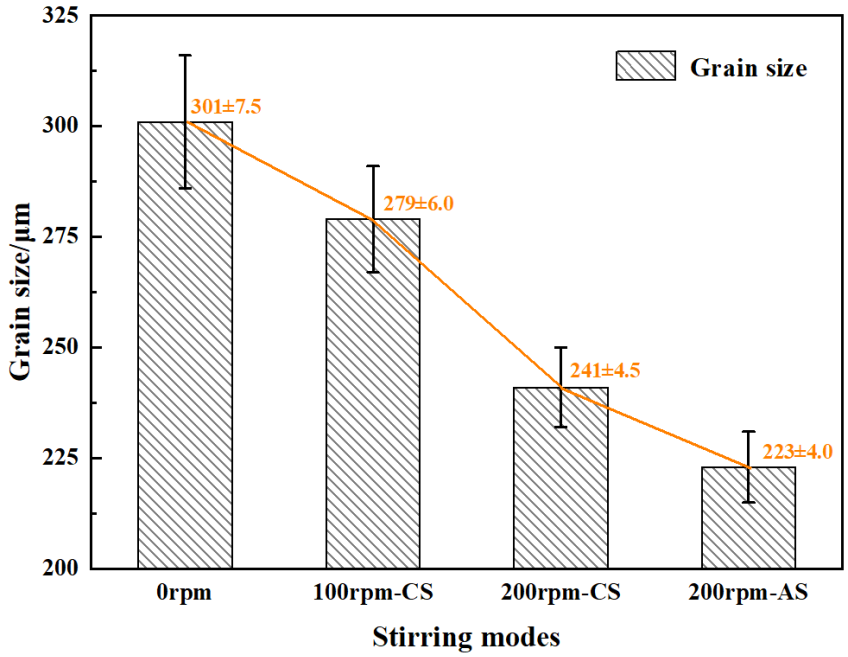

Figure 11. Comparison of grain size of ingot samples under different stirring modes: CS—continuous stirring; AS—alternate stirring.

According to the results in Figures 10 and 11, when the magnetic field was stationary, the molten alloy was also in a static state during solidification. The growth of columnar dendrites only stops when the temperature gradient disappears or they come into contact with each other, which is the reason for the large size during the stationary magnetic field. When the magnetic field moves in a circular direction, the Lorentz force drives the molten alloy in the crucible to move. The moving molten alloy cuts the primary dendrites, thereby shortening the length of the dendrites and refining the grain size. After the molten alloy flows stably, the dendrites tend to grow in the upstream direction, so a larger force is required to cut off the dendrites. That is the reason why the grain size in the sample was smaller at 200 rpm than at 100 rpm under the continuous stirring mode of the magnetic

field. When the magnetic field adopted an alternate stirring mode, the dendrites were cut off when the molten alloy rotated counterclockwise, and the broken position of the dendrite continued to generate new dendrites in the original direction during the stop stirring period. Because of the poor stability of the primary dendrites, when the flow direction of the molten alloy changes, the dendrites move in the opposite direction, which is easier to cut off. When there is continuous change in the molten alloy, more fractured dendrites are generated inside, providing conditions for the formation of fine and dense grains. The influence of different magnetic field stirring modes on the dendrite's growth in the ingot is shown in Figure 12.

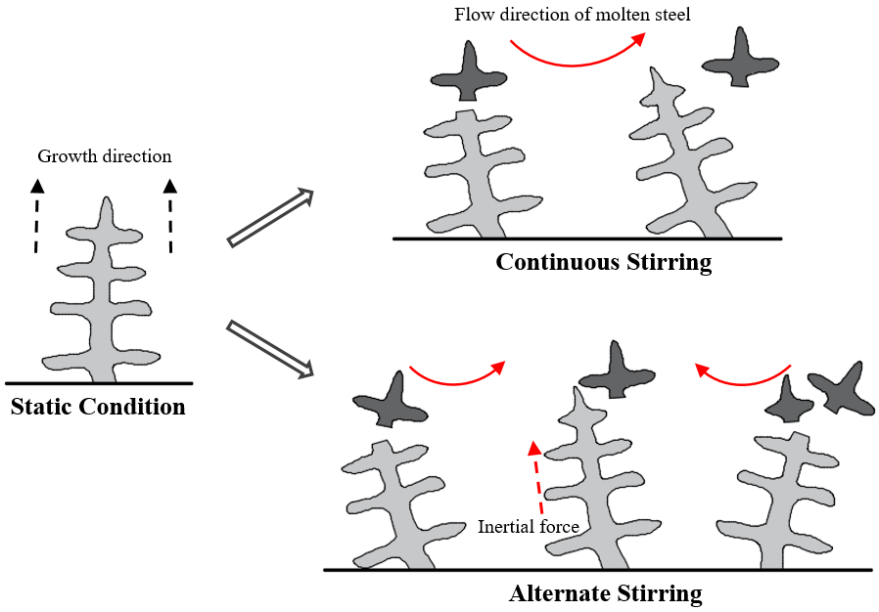

Figure 12. Schematic diagram of effect on dendrite growth in the ingot under different magnetic field stirring modes.

4.3. Distribution of Sn Element Inside Ingots

Sn-20 wt-% Pb alloy was used instead of steel in the experiment. Owing to the density difference between the Sn and Pb elements, during their solidification process, the Pb element tends to accumulate towards the bottom of the crucible under the action of gravity. Hence, the uniformity of element distribution can be judged by detecting the element content at different positions of the ingot. The morphology of the bottom of the ingots is shown in Figure 13.

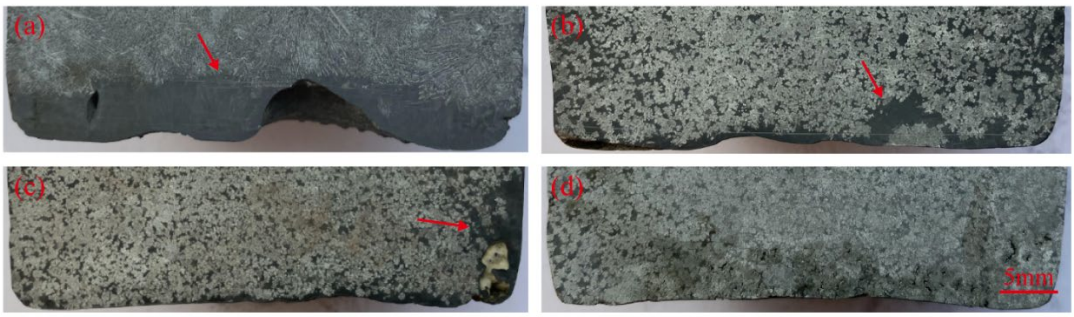

Figure 13. Morphology of the bottom of the ingots under different stirring modes: (**a**) 0 rpm; (**b**) continuous stirring, 100 rpm; (**c**) continuous stirring, 200 rpm; (**d**) alternate stirring, 200 rpm.

As can be seen from Figure 13, when the magnetic field was stationary, the molten alloy solidified under undisturbed conditions. Because of its high density, a large amount of Pb element accumulates at the bottom of the ingot, with a thickness of about 7 mm

(as shown by the red arrow). The magnetic field adopted the continuous stirring mode, and the molten alloy in the crucible rotated together under the action of the Lorentz force. The Pb element at the bottom of the ingot diffused under the action of centrifugal force. When the magnetic stirring speed was 100 rpm, the Pb element accumulation thickness at the bottom of the ingot decreased significantly to about 2 mm, but there was a certain degree of Pb element aggregation trend at the corner. When the stirring speed was 200 rpm, the thickness of the Pb element at the bottom of the ingot was further reduced to 0.7 mm, and meanwhile, obvious Pb clusters began to appear at the corner of the ingot. When the alternate stirring mode was used, the Pb element at the bottom of the ingot disappeared and the clusters at the corner were broken up. It can be concluded that when the magnetic field was stationary, the element uniformity in the ingot was the worst, while when the magnetic field adopted the alternate stirring mode and the stirring speed was 200 rpm, the element uniformity in the ingot was the best.

To quantitatively analyze the influence of different magnetic field stirring modes on the element uniformity in the ingots, an X-ray fluorescence spectrometer was used to detect the element distribution on the cross- and longitudinal sections of the ingots. The X-ray intensity of each element in the sample is not only related to the energy and intensity of the excitation source, but also to the content of each element. Based on the X-ray intensity of each element, the content information of the element can be obtained, which is the principle of XRF technology for detecting the element content in the sample. To ensure the accuracy of the detection results, the X-ray fluorescence spectrometer needs to be calibrated using standard samples before use. The test results for the ingots under different magnetic stirring modes are shown in Table 4 and Figure 14.

Table 4. Detection results for ingots under different magnetic stirring modes, %.

	H1	H2	H3	H4	H5	Z1	Z2	Z3	Z4	Z5
0 rpm	84.2	84.9	83.7	84.6	84.7	88.5	87.5	83.7	81.1	65.0
100 rpm-CS	79.9	85.1	85.8	84.9	80.3	88.3	86.6	85.8	83.2	77.6
200 rpm-CS	82.1	85.7	86.2	85.2	81.8	87.7	86.2	86.2	84.7	82.4
200 rpm-AS	84.8	85.9	86.2	86.5	84.6	86.7	85.3	86.8	86.2	85.3

According to the analysis of Figure 14a, when the magnetic field was static and the alternate stirring mode was used at 200 rpm, the fluctuation of the Sn element at different detection points on the cross-section of the ingots was small, that is, the uniformity was better. When the continuous stirring mode was adopted for the magnetic field and the stirring speeds were 100 rpm and 200 rpm, the central position of the Sn element in the cross-section of the ingots was high, with the composition of 85.8% and 86.2%, respectively. At the edge of the ingots, the content of Sn element showed a significant downward trend, with the proportions decreasing to 79.9% and 81.8%, respectively.

It can be seen from Figure 14b that when the magnetic field was stationary, the proportion of Sn element content in the ingot decreased from 88.5% to 65.0% from the top to the bottom. With the continuous stirring of the magnetic field, the uniformity of the Sn element in the longitudinal direction of the ingot gradually improved. When the magnetic field adopted the continuous stirring mode and the stirring speed was 100 rpm and 200 rpm, the proportion of the Sn element at the top and bottom of the ingots was 88.3% to 77.6% and 87.7% to 82.4%, respectively. With the magnetic field using an alternate stirring mode and a speed of 200 rpm, the longitudinal uniformity of the Sn element in the ingot was the best, and the proportion of Sn element at the top and bottom was 86.7% to 85.3%. The above results are consistent with the observation results presented in Figure 13. This indicates that in this study, when the alternate stirring mode was adopted and the speed was 200 rpm, the element uniformity inside the ingot was the best.

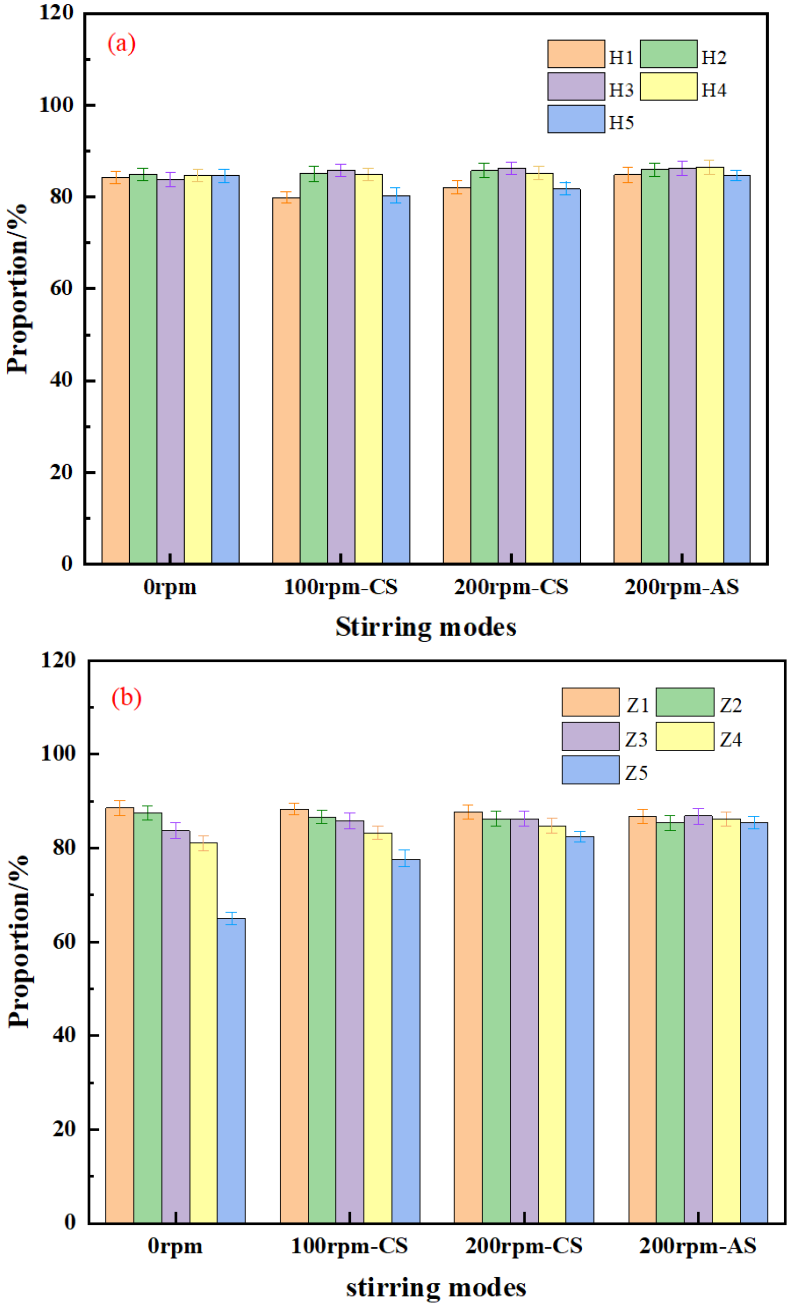

Figure 14. Distribution of Sn element in the center of ingots under different stirring modes: (**a**) cross-section; (**b**) longitudinal section.

5. Conclusions

In this paper, a permanent magnet stirrer was developed instead of an electromagnetic stirrer, and Sn-20%Pb alloy was used instead of steel. Furthermore, the effects of different magnetic field stirring modes on the solidification structure and element uniformity of the alloy ingots were studied. By comparing the macroscopic morphology, solidification structure, and uniform distribution of the elements under different magnetic stirring modes, the following conclusions were obtained:

(1) When the alternate stirring mode of the magnetic field was adopted, it obviously stabilized the molten alloy in the crucible. The flutter height at the ingot edge reduced from 4.12 mm to 1.86 mm after the magnetic field was adjusted from the continuous to alternate stirring mode with a speed of 200 rpm.

(2) When the alternate stirring mode of the magnetic field was adopted, it obviously shortened the grain size in the ingot and improved its compactness. When the magnetic field was stationary, the average grain size was about 301 μm. The magnetic field stirring speed was set to 200 rpm, and the corresponding grain size for the continuous stirring and alternate stirring modes were 241 μm and 223 μm, respectively.
(3) When the magnetic field was stationary, the Pb element was deposited at the bottom of the ingot, and the proportion of Sn element at the top and bottom of the ingot was 88.5% to 65.0%. With the circular motion of the magnetic field, the uniformity of the elements in the ingots was improved. When the magnetic alternate stirring mode was adopted, the proportion of Sn element at the top and bottom of the ingot was 86.7% and 85.3%, which greatly improved the uniformity of the element distribution inside the ingot.
(4) Regarding circular ingots, the magnetic alternate stirring mode can significantly improve the quality of the ingot. It can be further envisioned that in the continuous casting of round billet, the alternate electromagnetic stirring mode could be used in the production process to improve the internal quality of the billet.

Author Contributions: Writing—original draft preparation, M.Z.; Project administration, M.Z.; Resources, M.Z.; Funding acquisition, Y.B.; Investigation, Y.B.; Methodology, Y.B.; Software, H.Z.; Validation, H.Z. All authors have read and agreed to the published version of the manuscript.

Funding: This research received no external funding.

Data Availability Statement: Not applicable.

Conflicts of Interest: No potential conflicts of interest are reported by the authors.

References

1. Zhou, J.; Zhu, L.; Sun, L.; Wang, B.; Xiao, P. Analysis of the Formation Mechanism of Surface Cracks of Continuous Casting Slabs Caused by Mold Wear. *Processes* **2022**, *10*, 797. [CrossRef]
2. Yang, B.; Wang, M.; Zhang, H.; Liu, S.; Wang, G.; Wang, X. Optimization of Heavy Reduction Process on Continuous-Casting Bloom. *Metals* **2022**, *12*, 1873. [CrossRef]
3. Li, X.; Wang, X.; Bao, Y.; Gong, J.; Pang, W.; Wang, M. Effect of Electromagnetic Stirring on the Solidification Behavior of High-Magnetic-Induction Grain-Oriented Silicon Steel Continuous Casting Slab. *JOM* **2020**, *72*, 3628–3633. [CrossRef]
4. Han, Y.-S.; Yan, W.; Zhang, J.-S.; Chen, J.; Chen, W.-Q.; Liu, Q. Comparison and integration of final electromagnetic stirring and thermal soft reduction on continuous casting billet. *J. Iron Steel Res. Int.* **2020**, *28*, 160–167. [CrossRef]
5. Arh, B.; Tehovnik, F.; Plostajner, H. The influence of the electromagnetic stirring on macro and microstructure of the continuously casting billets. *Metalurgija* **2005**, *44*, 305–310.
6. Cong, J.; Wang, H.; Ling, H.; Yang, J.; Hu, P.; Zhang, X. The research on internal crack formation and solving in billet during soft reduction. *Met. Res. Technol.* **2017**, *114*, 517. [CrossRef]
7. Zou, J.; Zhang, H.; Wu, Z.; Wang, J.; Li, B.; Cui, J.; Nagaumi, H.; Li, Y. Effects of an intermittent permanent magnet stirring on the melt flow and grain refinement of Al–4.5Cu alloy. *J. Mater. Res. Technol.* **2021**, *14*, 1585–1600. [CrossRef]
8. Ma, H.; Zhang, J.; Yin, Y.; Yan, Z.; Liu, H. Numerical simulation on the central macro-segregation during billet continuous casting with the soft reduction. *Ironmak. Steelmak.* **2022**, *49*, 887–897. [CrossRef]
9. Geng, X.; Li, X.; Liu, F.B.; Li, H.B.; Jiang, Z.H. Optimization of electromagnetic stirring parameters for round billet continuous casting molds. *J. Cent. South Univ.* **2015**, *46*, 4411–4416.
10. Guoping, L.; Yaoguang, W.; Jianping, Z. Research on effect of mold electromagnetic stirring on quality of round billets. *Iron. Steel.* **2005**, *40*, 30–32,53.
11. Wu, C.; Wang, Q.; Li, D.; Zhu, X.; Jin, B.; Wang, L.; Lei, H. Macro-segregation under new flow pattern and temperature distribution induced by electromagnetic swirling flow in nozzle during continuous casting of square billet. *J. Mater. Res. Technol.* **2020**, *9*, 5630–5639. [CrossRef]
12. Li, J.B.; Deng, B.R.; Yang, X.Z.; Liang, L.; Wang, H.C.; Wu, T. Microstructure control of continuous casting slab of grain oriented silicon steel. *Mater. Trans.* **2022**, *63*, 112–117. [CrossRef]
13. Li, S.; Han, Z.; Zhang, J. Numerical Modeling of the Macrosegregation Improvement in Continuous Casting Blooms by Using F-EMS. *JOM* **2020**, *72*, 4117–4126. [CrossRef]
14. Jiang, D.-Q.; Wang, R.; Zhang, Q.; Zhang, Z.-Q.; Tu, T.-S.; Wang, J.; Ren, Z.-M. Effect of final electromagnetic stirring on solidification microstructure of GCr15 bearing steel in simulated continuous casting. *J. Iron Steel Res. Int.* **2020**, *27*, 141–147. [CrossRef]

15. Nick, A.S.; Vynnycky, M. On longitudinal electromagnetic stirring in the continuous casting of steel blooms. *J. Eng. Math.* **2020**, *120*, 129–151. [CrossRef]
16. An, H.; Bao, Y.; Wang, M.; Zhao, L. Effects of electromagnetic stirring on fluid flow and temperature distribution in billet continuous casting mould and solidification structure of 55SiCr. *Met. Res. Technol.* **2017**, *115*, 103. [CrossRef]
17. Yu, H.Q.; Zhu, M.Y. Influence of electromagnetic stirring on transport phenomena in round billet continuous casting mould and macrostructure of high carbon steel billet. *Ironmak. Steelmak.* **2012**, *39*, 574–584. [CrossRef]
18. Jiang, D.; Wang, R.; Zhu, L.; Zhang, Q.; Li, C.; Wang, J.; Ren, Z. Thermal and numerical simulation of mould electromagnetic stirring of GCr15 bearing steel. *Mater. Sci. Technol.* **2019**, *35*, 2173–2180. [CrossRef]
19. Yang, B.; Deng, A.-Y.; Li, Y.; Xu, X.-J.; Wang, E.-G. Numerical simulation of flow and solidification in continuous casting process with mold electromagnetic stirring. *J. Iron Steel Res. Int.* **2018**, *26*, 219–229. [CrossRef]
20. Xia, Y.; Li, L.; Wang, P.; Tie, Z.-P.; Lan, P.; Tang, H.-Y.; Zhang, J.-Q. Characteristics of the as-cast high-carbon micro-alloyed continuous casting bloom steel for expansion-break connecting rods. *Chin. J. Eng.* **2022**, *44*, 189–197.
21. Zhan, N.; Hu, Z.; Zhang, X. Experimental Investigation of Fatigue Crack Growth Behavior in Banded Structure of Pipeline Steel. *Metals* **2020**, *10*, 1193. [CrossRef]
22. Cheng, C.G.; Liu, Z.T.; Wan, W.C.; Zheng, Y.R.; Di, Y.T. Study on Formation Mechanism of Frame-Shaped Segregation in 40Cr Wire Rod Rolled from Bloom. *Adv. Mater. Res.* **2011**, *402*, 211–214. [CrossRef]
23. He, X.; Wang, X.; Wang, Y.; Meng, Y. Formation and effects of banded structures in 55SiCrA spring steel wire rod. *Met. Res. Technol.* **2015**, *112*, 606. [CrossRef]
24. Zhang, Z.; Wu, M.; Zhang, H.; Hahn, S.; Wimmer, F.; Ludwig, A.; Kharicha, A. Modeling of the as-cast structure and macrosegregation in the continuous casting of a steel billet: Effect of M-EMS. *J. Mater. Process. Technol.* **2022**, *301*, 117434. [CrossRef]
25. Wang, P.; Tie, Z.; Li, S.; Lan, P.; Tang, H.; Zhang, J. Effect of M-EMS current intensity on the subsurface segregation and internal solidification structure for bloom casting of 42CrMo steel. *Ironmak. Steelmak.* **2021**, *48*, 779–787. [CrossRef]
26. Huo, Y.-K.; Zhao, L.-H.; An, H.-H.; Wang, M.; Zou, C.-D. Model prediction of the effect of in-mold electromagnetic stirring on negative segregation under bloom surface. *Int. J. Miner. Met. Mater.* **2020**, *27*, 319–327. [CrossRef]
27. Wang, P.; Xiao, H.; Shen, H.; Chen, X.; Chen, L.; Lan, P.; Zhang, J. Effect of mold electromagnetic stirring on the gear steel solidification behavior of its large-sized round casting. *J. Mech. Eng.* **2021**, *57*, 105–111.
28. Lijima, Y.; Kakehi, K. Effect of Pb on the mechanical properties of Inconel 718. *J. Jpn. I Met. Mater.* **2014**, *78*, 201–204.
29. Jiang, Y.; Zhao, J.; Sun, L.; Gong, H.; Gong, X. Effects of alloying elements on cohesion and brittleness of grain boundary of iron. *Mater. Chem. Phys.* **2022**, *275*, 125291. [CrossRef]

Disclaimer/Publisher's Note: The statements, opinions and data contained in all publications are solely those of the individual author(s) and contributor(s) and not of MDPI and/or the editor(s). MDPI and/or the editor(s) disclaim responsibility for any injury to people or property resulting from any ideas, methods, instructions or products referred to in the content.